APL Materials

Substrate-orientation dependence of β-Ga$_2$O$_3$ (100), (010), (001), and ($\bar{2}$01) homoepitaxy by indium-mediated metal-exchange catalyzed molecular beam epitaxy (MEXCAT-MBE) Ⓕ

P. Mazzolini ⬛, A. Falkenstein ⬛, C. Wouters ⬛, R. Schewski ⬛, T. Markurt, Z. Galazka ⬛, M. Martin ⬛, M. Albrecht ⬛, and O. Bierwagen ⬛

COLLECTIONS

Ⓕ This paper was selected as Featured

View Online   Export Citation   CrossMark

ARTICLES YOU MAY BE INTERESTED IN

A review of Ga$_2$O$_3$ materials, processing, and devices
Applied Physics Reviews **5**, 011301 (2018); https://doi.org/10.1063/1.5006941

Recent progress on the electronic structure, defect, and doping properties of Ga$_2$O$_3$
APL Materials **8**, 020906 (2020); https://doi.org/10.1063/1.5142999

Gallium oxide (Ga$_2$O$_3$) metal-semiconductor field-effect transistors on single-crystal β-Ga$_2$O$_3$ (010) substrates
Applied Physics Letters **100**, 013504 (2012); https://doi.org/10.1063/1.3674287
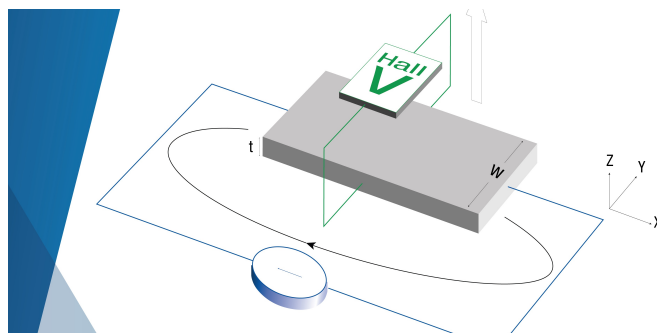
Substrate-orientation dependence of β-Ga₂O₃ (100), (010), (001), and (2̄01) homoepitaxy by indium-mediated metal-exchange catalyzed molecular beam epitaxy (MEXCAT-MBE) 🅕

P. Mazzolini,[1,a] 🆔 A. Falkenstein,[2] 🆔 C. Wouters,[3] 🆔 R. Schewski,[3] 🆔 T. Markurt,[3] Z. Galazka,[3] 🆔 M. Martin,[2] 🆔 M. Albrecht,[3] 🆔 and O. Bierwagen[1] 🆔

AFFILIATIONS

[1] Paul-Drude-Institut für Festkörperelektronik, Leibniz-Institut im Forschungsverbund Berlin e.V., Hausvogteiplatz 5–7, 10117 Berlin, Germany
[2] Institute of Physical Chemistry, RWTH Aachen University, D-52056 Aachen, Germany
[3] Leibniz-Institut für Kristallzüchtung, Max-Born-Str. 2, 12489 Berlin, Germany

a) mazzolini@pdi-berlin.de

ABSTRACT

We experimentally demonstrate how In-mediated metal-exchange catalysis (MEXCAT) allows us to widen the deposition window for β-Ga₂O₃ homoepitaxy to conditions otherwise prohibitive for its growth via molecular beam epitaxy (e.g., substrate temperatures ≥800 °C) on the major substrate orientations, i.e., (010), (001), (2̄01), and (100) 6°-offcut. The obtained crystalline qualities, surface roughnesses, growth rates, and In-incorporation profiles are shown and compared with different experimental techniques. The growth rates, Γ, for fixed growth conditions are monotonously increasing with the surface free energy of the different orientations with the following order: $\Gamma(010) > \Gamma(001) > \Gamma(2̄01) > \Gamma(100)$. Ga₂O₃ surfaces with higher surface free energy provide stronger bonds to the surface ad-atoms or ad-molecules, resulting in decreasing desorption, i.e., a higher incorporation/growth rate. The structural quality in the case of (2̄01), however, is compromised by twin domains due to the crystallography of this orientation. Notably, our study highlights β-Ga₂O₃ layers with high structural quality grown by MEXCAT-MBE not only in the most investigated (010) orientation but also in the (100) and (001) ones. In particular, MEXCAT on the (001) orientation results in both growth rate and structural quality comparable to the ones achievable with (010), and the limited incorporation of In associated with the MEXCAT deposition process does not change the insulating characteristics of unintentionally doped layers. The (001) surface is therefore suggested as a valuable alternative orientation for devices.

Driven by its application potential for high power electronics, gallium oxide in its most thermodynamically stable monoclinic structure, β-Ga₂O₃, has recently shown signs of rising interest from the scientific community.[1] Its successful implementation in devices requires high purity, low structural defectivity,[2] and the controlled incorporation of dopants at the nanoscale, all of which can be achieved by molecular beam epitaxy (MBE). A definitive advantage of β-Ga₂O₃ over its direct competitors in power electronics (e.g., SiC and GaN) is the possibility of growing the material from the melt.[3,4] This results in the availability of native gallium oxide

substrates with currently four different crystal orientations—i.e. (100), (001), (2̄01), and (010)—that enable the highest structural quality of Ga₂O₃ films by homoepitaxial growth. Despite the perfect crystalline match between substrate and film, the homoepitaxy of β-Ga₂O₃ still presents two major challenges. The first one is related to the peculiar structure of the respective growth surfaces[5] that can result in the formation of twin lamellae due to double positioning, i.e., the formation of 2D nuclei in twinned or true epitaxial relation as shown in (100)-homoepitaxy by metal organic vapor phase epitaxy (MOVPE)[6] and MBE.[7] These defects strongly deteriorate the

electrical properties of the deposited layers[8] but can be prevented by an appropriate offcut of the substrate as recently demonstrated by MOVPE (100)-homoepitaxy.[9] On (010)-oriented substrates, the symmetry of the growth surface prevents double positioning and thus twin formation. For the other available Ga_2O_3 orientations— i.e., (001) and ($\bar{2}$01)—systematic experimental work on the structural quality of the deposited layers is lacking so far. The second challenge is the limited growth rate during MBE of Ga_2O_3,[10,11] which is related to the peculiar two-step growth kinetics via the intermediate formation of the suboxide Ga_2O in the first step and its further oxidation to Ga_2O_3 in the second step.[12] As Ga_2O has a significantly higher vapor pressure than Ga,[13] its desorption limits the growth rate due to the following three factors: (1) metal-rich conditions, providing insufficient O-flux Φ_O to oxidize all formed suboxide,[14] (2) high substrate temperatures (T_g) at which the thermally activated desorption of Ga_2O outperforms its oxidation even under O-rich growth conditions,[15] and (3) β-Ga_2O_3 substrate orientations that provide only weak bonds to the adsorbed Ga_2O, resulting in a low activation energy for its desorption. In fact, surfaces with higher stability (i.e., cleavage planes) such as (100) and (001) have been found to suffer from very limited growth rates with respect to noncleavage planes such as (010) during MBE,[10,16] while MOVPE evidences almost identical growth rates for β-Ga_2O_3 homoepitaxy on different substrate orientations.[17]

For these reasons, the homoepitaxy of β-Ga_2O_3 by MBE has so far been mostly restricted to the (010) orientation and growth conditions that are not limiting its growth rate (e.g., O-rich, T_g < 800 °C).[10,16] In contrast, metal-rich deposition conditions are predicted to avoid the formation of gallium vacancies (acting as compensating deep acceptors)[18,19] and higher T_g generally result in higher crystalline quality and allows us to increase the stability range of β-$(Al_xGa_{1-x})_2O_3$ alloys.[20] Moreover, substrate orientations other than (010) are desirable to mitigate the following drawbacks: (i) the (010) surface has been shown to be unstable under metal-rich growth conditions, i.e., resulting in the formation of (110)-facets,[21] and (ii) it is not a cleavage plane and therefore currently more challenging to be prepared[22] with respect to the (001), ($\bar{2}$01), and (100) surfaces, at least without considering the possible need of defined substrate offcuts.[9] Consequently, there is a need to increase the growth rate for crystal orientations other than (010) and interest in exploring growth conditions that so far have prevented layer growth by MBE, i.e., high T_g and metal-rich conditions.

MBE growth using metal-exchange catalysis[23,24] (MEXCAT) is a promising avenue to overcome these limitations. This process is based on the collaborative effect of kinetically favored formation of intermediate In_2O_3 (which can grow at lower O-flux and higher T_g than Ga_2O_3)[13,14] and the subsequent thermodynamically driven exchange of its In-atoms by Ga (due to stronger Ga–O than In–O bonds).[25] In-mediated MEXCAT-MBE has been shown to enable a high Ga_2O_3 growth rate with limited In-incorporation under conditions (Ga-rich, high T_g) prohibitive for growth of Ga_2O_3 due to severe Ga_2O desorption.[23] Likewise, Sn-flux mediated Ga_2O_3 heteroepitaxy by MEXCAT-MBE[24] lead to the same qualitative results, demonstrating the generality of the MEXCAT approach for MBE. Both Sn- and In-mediated MEXCAT-MBE performed on top of a buffer layer of ($\bar{2}$01)-oriented β-Ga_2O_3 on c-plane sapphire substrates resulted in the formation of the metastable ε/κ-phase of

Ga_2O_3.[23,24,26] Recently, In-mediated MEXCAT on β-Ga_2O_3 (010) substrates has been demonstrated to triple the Ga_2O_3 growth rate under Ga-rich conditions at T_g = 900 °C, preserve the monoclinic structure, and maintain a low surface roughness (rms <0.5 nm) while limiting the In-incorporation (not detectable X-ray diffraction XRD peak shift and no In-signal from energy dispersive x-ray spectroscopy EDX).[21] Furthermore, the concept of In-mediated MEXCAT has been extended to the deposition of β-$(Al_xGa_{1-x})_2O_3$ alloys on (010) substrates, allowing for stabilization of up to x = 0.2 incorporation at high T_g.[20]

In this experimental work, we investigate the In-mediated MEXCAT on all the available orientations of β-Ga_2O_3 substrates, aiming at insights in the crystal quality and future perspective of Ga_2O_3 homoepitaxy by MBE on different surfaces. In particular, we show that MEXCAT allows for homoepitaxial growth under deposition conditions otherwise prohibitive on all the major β-Ga_2O_3 orientations. The synthesis parameters that allow for layer growth (i.e., T_g, O/Ga-flux ratio) as well as the growth rates are found to depend on the surface orientation, which we explain by the relation between surface free energy from *ab initio* calculations (Ref. 9) and ad-atom binding energy extracted from our data using the growth model for MEXCAT-MBE presented in Ref. 23. Furthermore, we show that the ($\bar{2}$01)-orientation is challenging for β-Ga_2O_3 homoepitaxy due to the formation of twins. MEXCAT, however, allows for the homoepitaxy of high quality β-Ga_2O_3 layers on both (100) 6°-offcut and (001) substrates (no structural defects identified, rms < 0.5 nm), with low In incorporation (In < 0.1 cation cat. %). In particular, the (001)-orientation also allowed for growth rates comparable to the ones obtainable in (010) homoepitaxy (i.e., 2.3 nm/min).

The ($\bar{2}$01) and (010) β-Ga_2O_3 orientated substrates for this study were unintentionally doped and Fe-doped, respectively, and were both purchased from the Tamura company, while the (100) and (001) oriented wafers were Mg-doped and prepared from bulk crystals obtained from the Czochralski method[4] at the Leibniz-Institut für Kristallzüchtung. To prevent the formation of twin domains, the (100)-substrates were offcut by 6° toward the -c direction.[9] Before being loaded into the MBE chamber, the substrates were chemically etched in phosphoric acid (85 wt. % H_3PO_4, T = 130 °C, t = 15 min) to remove potential polishing damage in the first 100 nm from the substrate surface;[27] the process was then followed by an O_2-annealing treatment (p = 1 bar, T = 950 °C, t = 60 min) in a tube furnace. The experiments were performed in a MBE chamber equipped with an O-plasma source run at a plasma power P = 300 W. Before the deposition, all the substrates were *in situ* oxygen-plasma treated at an O-flux of 1 standard cubic centimeter per minute (sccm) at a substrate temperature T_g = 875 °C for t = 30 min. All growth runs were performed for a fixed deposition time of 30 min. The beam equivalent pressure of Ga was fixed to BEP_{Ga} = 1.27 × 10^{-7} mbar, equivalent to a particle flux of Φ_{Ga} = 2.2 nm^{-2} s^{-1} (determined from the measured growth rate under O-rich deposition conditions on c-plane sapphire substrates[14])— i.e., full Ga incorporation ≈100 nm (i.e., growth rate 3.3 nm/min). The particle flux of In for the catalyzed growths was fixed to Φ_{In} = 1/3 Φ_{Ga} (BEP_{In} = 5.2 × 10^{-8} mbar). The T_g was measured by an optical pyrometer. For some of the depositions, an additional thin $(Al_xGa_{1-x})_2O_3$ marker layer was deposited at the substrate-layer interface. The growth parameters for the interlayer were maintained

the same regardless of the different investigated surfaces, with T_g = 720 °C, an O-flux of 1 sccm, Al cell temperature = 1008 °C (BEP_{Al} ≈ 4 × 10^{-8} mbar), and deposition time = 80 s (targeted Al composition ≈ 5 cat. %, thickness ≈ 1–5 nm). The surface morphology was characterized by atomic force microscopy (AFM, Bruker Dimension Edge) in PeakForce tapping mode. The homoepitaxial layers were monitored by XRD symmetric, out-of-plane 2θ-ω scans (PANalytical X'Pert Pro MRD using Cu K$_α$ radiation), and their composition was investigated by means of time-of-flight secondary ion mass spectrometry (SIMS) using ToF-SIMS IV from IONTOF GmbH. The quantitative ToF-SIMS calibration of the In-concentration was obtained from pulsed laser deposited $(In_xGa_{1-x})_2O_3$ reference films on c-plane sapphire substrates analyzed by EDX in a scanning electron microscope (5 samples with In content 1–40 c at. %—Oxford Instruments GmbH/JEOL GmbH). Depth profiling of SIMS craters was performed by interference microscopy (Veeco Instruments, Inc.). Selected samples were investigated by transmission electron microscopy (TEM—aberration corrected FEI Titan 80–300 operating at 300 kV). Scanning TEM (STEM) images were recorded with a high-angle annular dark-field (HAADF) detector with an inner acceptance angle of 35 mrad and a camera length of 196 mm. TEM samples were prepared and studied in the cross section view perpendicular to the [010] direction for the (100), (001), and ($\bar{2}$01) growth orientations.

We initially applied on all the substrate orientations the nominal deposition parameters that we previously reported to be effective for the In-mediated MEXCAT-MBE of (010)-oriented layers, i.e.,

Tg = 900 °C, Φ_{In} = 1/3 Φ_{Ga}, and O-flux = 0.33 sccm.[21] With the formation of (110)-facets, the resulting (010)-homoepitaxial layer shows the typical morphology previously highlighted for metal-rich deposition conditions (see Ref. 21). Its thickness of 50 nm (detected by XRD thickness fringes, not shown) signifies an effective incorporation of ≈50% of the incoming Ga flux; the thickness reduction with respect to what we have previously reported[21] can be attributed to a slightly different efficiency of our O-plasma source. More importantly, no layer growth was detected on all the other substrate orientations (not shown), indicating a substrate-orientation dependence of In-mediated MEXCAT for β-Ga_2O_3 homoepitaxy. The mean surface roughness of the substrates after these growth experiments are reported in Tables I–III for ($\bar{2}$01), (100), and (001), respectively. We point out that when no growth takes place, the rms values might be altered by localized Ga-etching effects that cause a roughening of the surfaces with respect to an untreated substrate.

In the following, we report the results of growth on the different substrate orientations under various growth conditions (T_g, O-flux).

MEXCAT on ($\bar{2}$01). Growth of homoepitaxial layers on this substrate orientation was found to require much lower T_g and/or higher O-fluxes with respect to the (010) one. A decrease of T_g down to 735 °C resulted in a rough morphology (rms = 2.45 nm) characterized by elongated features oriented along the [010] direction [Fig. 1(a)].

The cross-sectional STEM HAADF images of this sample [Figs. 1(b) and 1(c)] confirm the growth of a ($\bar{2}$01) homoepitaxial layer and allow us to relate its AFM morphology to the presence
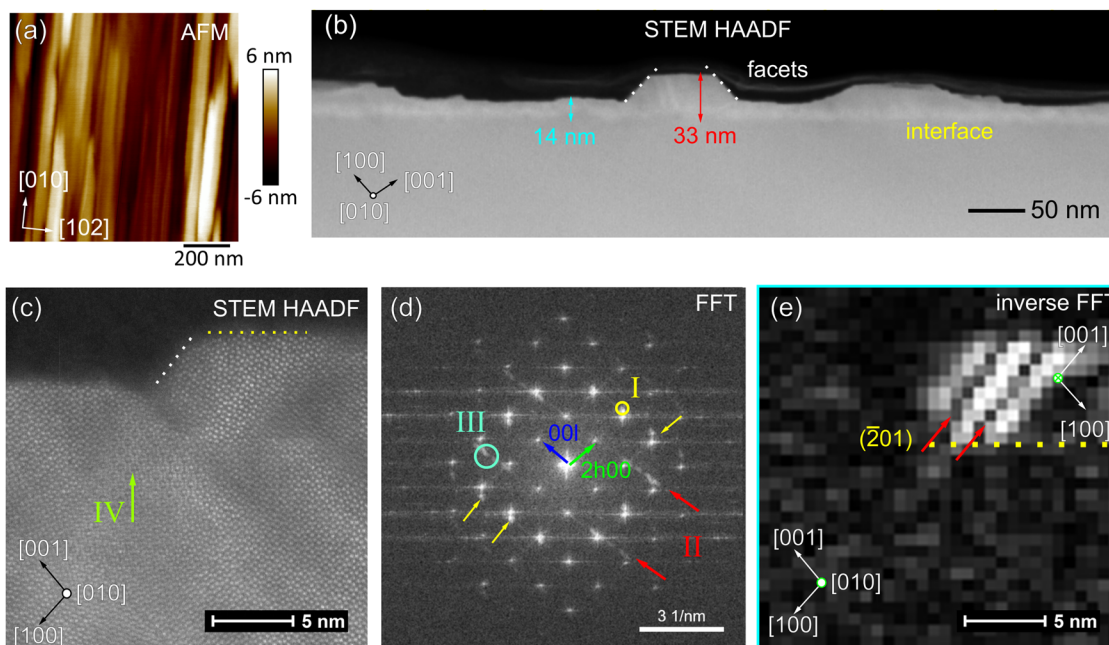

FIG. 1. (a) AFM micrograph of ($\bar{2}$01) oriented layers deposited with an O-flux = 0.33 sccm at T_g = 735 °C with In-catalysis. (b) Cross-sectional STEM HAADF image of the layer projected along the b direction of the monoclinic lattice. (c) High resolution STEM HAADF images of the same layer. In this image, bright spots correspond to the positions of Ga (Z = 31) columns, while oxygen (Z = 8) columns are not visible due to the difference in the atomic number. (d) FFT of the HR STEM image. The direction of the 00l and 2h00 reflections of the substrate are marked by the blue and green arrows, respectively. Extra reflections and streaks are marked by the yellow and red arrows. (e) Inverse FFT of (d) taking solely the region marked with the circle at position (III).

of islands along the [010] direction. Due to the irregular height and distribution of the islands, it is difficult to identify a precise layer thickness (range 15–30 nm, i.e., ≈20% incorporation of the incoming Ga-flux). Under these deposition conditions, the presence of well-defined facets on the side of the islands [white dotted lines in Fig. 1(b)] is visible. Figure 1(c) shows an atomically resolved STEM HAADF image of a part of an island, which reveals three kinds of defects, i.e., twin lamellae on the $(\bar{2}01)$ plane, twins on the (100) plane, and a defect induced by a lateral shift of a part of the layer with respect to the other on the $(\bar{2}01)$ growth surface. All of these defects can be explained by the 2D-island growth on the respective growth surfaces. Evidence for these defects comes from the analysis of Fast Fourier Transformations (FFTs) of Fig. 1(c) [Fig. 1(d)] and corresponding inverse FFTs. The extrareflections (I) and the streaks (II) in the FFT [Fig. 1(d)] correspond to a twinning of the lattice on the $(\bar{2}01)$ plane and are revealed by high intensity in the inverse FFT in Fig. 1(e) [inverse FFT extracted from region (III) in Fig. 1(d)]. Within this twinned island, additional twins on the (100) planes appear as dark lines. These dark lines correspond to half unit cell high twin lamellae.[28] The image pattern in the region marked IV [green arrow Fig. 1(c)] has already been observed in homoepitaxial layers grown on the (100) plane of β-Ga_2O_3.[29] It is explained by the overlap of two different grains, whose lattices have been shifted in the $(\bar{2}01)$ plane with respect to each other.

The ToF-SIMS measurement performed on a twin sample deposited under the same conditions independently confirms the presence of a layer consisting of islands with broad height distribution, as visible from the double-peak in the In-intensity profile [red dots in Fig. 2(a)]. From the calibration, the In-concentration in this sample is found to be around C_{In} ≈ 2 × 10^{19} cm^{-3} [i.e., ≈0.05 cat. %] at a depth of x ≈ 5 nm. Si impurities are usually found as a contaminant in Ga_2O_3 homoepitaxy at the substrate-layer interface[30] and can therefore be used as an interface marker [blue dots in Fig. 2(a)]. The absence of a second Si-peak at ≈20 nm is related to its lower intensity with respect to the In one (near the detection limit). The layer thickness can be estimated around 10–25 nm from the SIMS profile, in line with TEM results [Fig. 1(b)].

For comparison, another layer was deposited under the very same conditions (i.e., T_g = 735 °C and O-flux = 0.33 sccm) without providing an additional In-flux. The SIMS profile of this sample [Fig. 2(b)] shows Si impurities only at the surface, clearly indicating the absence of a deposited layer. Since no In-flux was provided
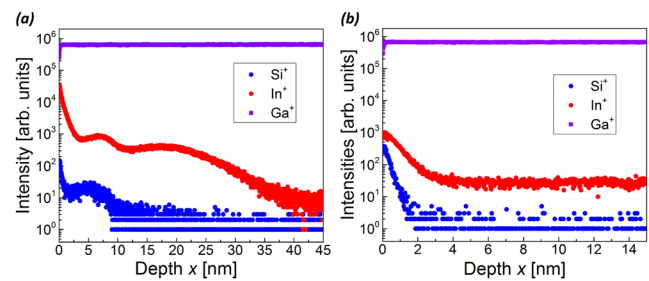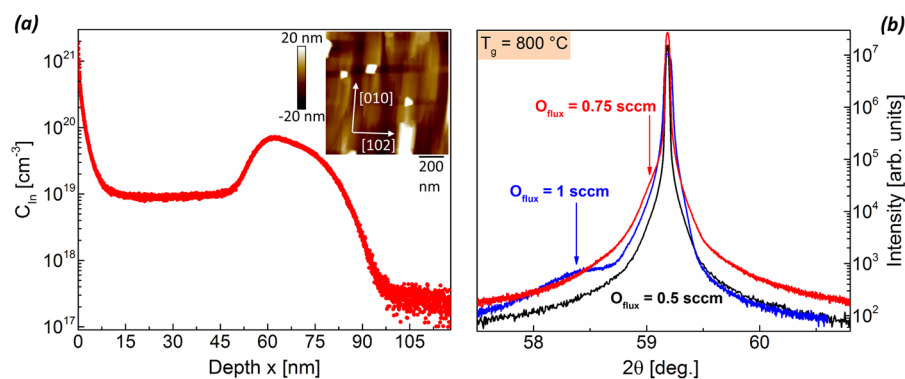

FIG. 2. ToF-SIMS of $(\bar{2}01)$ homoepitaxial layers deposited at T_g = 735 °C with an O-flux = 0.33 sccm (a) with In-mediated MEXCAT and (b) without additional In-flux.

during this growth run, the presence of a certain amount of In in the first nanometers of the substrate (C_{In} ≈ 2 × 10^{19} cm^{-3}) has to be considered as a surface impurity most likely coming from the sample holder, which has been the same for all the deposition runs.

Further deposition conditions were screened aiming at improving the quality of the homoepitaxial $(\bar{2}01)$ layers. In-catalyzed growth with an increased O-flux of 0.5 sccm resulted in a nonhomogeneous rough surface (rms = 9.81 nm) with high incorporation of the incoming Ga-flux (≈85 nm thick layer, not shown) and C_{In} ≈ 5 × 10^{20} cm^{-3} (i.e., ≈1.3 cat. %, not shown). Increasing incorporation of In with increasing O-flux and/or decreasing T_g has already been reported for the heteroepitaxy of $(In_xGa_{1-x})_2O_3$.[25]

A higher T_g of 800 °C required to increase the O-flux up to 0.75 sccm to detect layer growth with In-catalysis (i.e., no growth detected for 0.33 and 0.5 sccm). With these growth conditions, a 60–70 nm layer was deposited: the C_{In} as a function of probed depth [Fig. 3(a)] shows that after an intial broad peak detected at the substrate-layer interface (max C_{In} ≈ 7.2 × 10^{19} cm^{-3}, i.e., ≈0.19 cat. %), the C_{In} stabilizes to a value of ≈9.8 × 10^{18} cm^{-3}, i.e., ≈0.03 cat. %. The presence of an In-peak at the substrate-layer interface has been generally identified in all the samples and is probably related to the first stages of the catalytic growth. An AFM image of this sample [inset of Fig. 3(a)] shows a rough surface (rms = 6.99 nm) dominated by islands oriented along the [010] direction, similarly to the ones shown in Fig. 1(a). A reference sample deposited without In-catalysis under the very same growth conditions resulted in no layer growth (not shown).

FIG. 3. (a) ToF-SIMS In concentration profile of a $(\bar{2}01)$ homoepitaxial layer deposited at T_g = 800 °C with an O-flux = 0.75 sccm with In-mediated MEXCAT; the AFM micrograph of the layer is shown in the inset of the graph. (b) XRD of the $(\bar{6}03)$ diffraction peaks of the layers deposited at T_g = 800 °C with different O-fluxes.
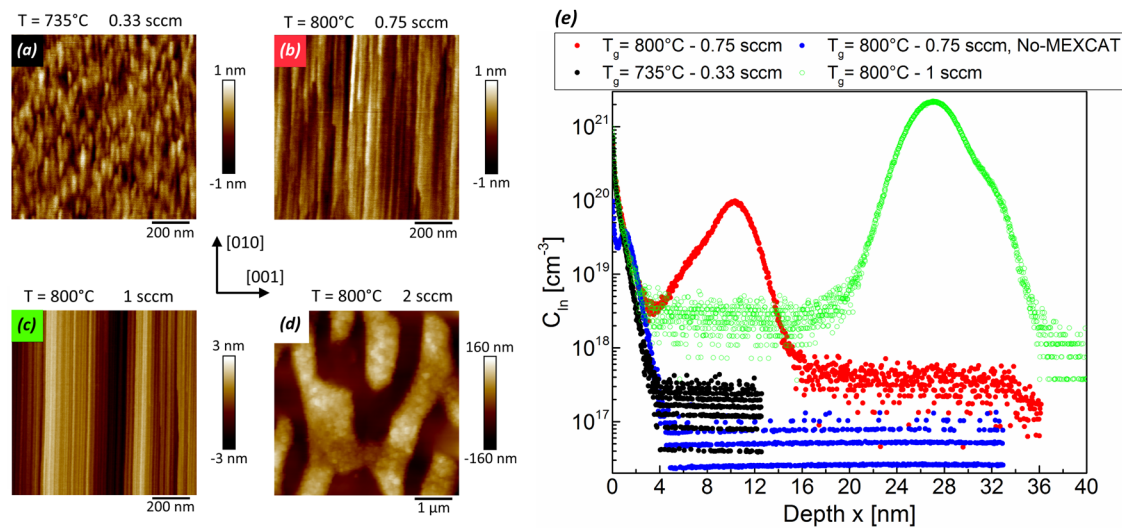
FIG. 4. AFM micrographs of samples deposited on 6° offcut (100) with In-mediated MEXCAT (a) at T_g = 735 °C, O-flux = 0.33 sccm and at T_g = 800 °C with (b) 0.75 sccm, (c) 1 sccm, and (d) 2 sccm O-fluxes. (e) ToF-SIMS In concentration profile of (a), (b), (c), and of a noncatalyzed sample deposited at T_g = 800 °C with 0.75 sccm O-flux (black, red, green, and blue dots, respectively).

A further increase of the O-flux to 1 sccm at T_g = 800 °C with In-catalysis resulted in almost full Ga-flux incorporation and a surface characterized by several micrometers large islands with an irregular shape and a typical height of ≈50–80 nm [similar morphology to Fig. 4(d)]. Also in this case, the increased O-flux resulted in significant In-incorporation into the layer (C_{In} up to 1.5×10^{21} cm^{-3}, i.e., ≈3.92 cat. %). In Fig. 3(b), we report the $(\bar{6}03)$ XRD peaks of catalyzed samples deposited at different O-fluxes at the same T_g of 800 °C; in line with the SIMS results, a larger O-flux induces a gradually higher incorporation of In in the form of the β-$(In_xGa_{1-x})_2O_3$ alloy (i.e., left-side shift of the β-Ga_2O_3 diffraction peak). In contrast to what has been previously reported in Ga_2O_3 heteroepitaxy on c-plane sapphire substrates with a $(\bar{2}01)$-oriented β-Ga_2O_3 seed layer,[23] In-mediated MEXCAT in $(\bar{2}01)$-homoepitaxy never

resulted in the formation of the metastable ε/k-phase[26] in our layers.

As summarized in Table I, we show that In-mediated MEXCAT allows us to widen the growth window in $(\bar{2}01)$ homoepitaxy to regimes otherwise prohibitive for β-Ga_2O_3 growth, enabling large Ga-flux incorporation (up to ≈65%) with limited In-incorporation (<0.1 cat. %). Nonetheless, our results suggest that obtaining $(\bar{2}01)$ layers with high structural quality would require a proper choice of the substrate offcut to prevent the formation of twin lamellae due to the possibility of double positioning during growth. Twin lamellae can limit the electrical transport properties and results in considerable surface roughness in our deposited layers.

MEXCAT on (100) 6°-offcut. The In-assisted synthesis conditions that allowed for growth at the lowest T_g for the $(\bar{2}01)$

TABLE I. Summary results for the $(\bar{2}01)$ homoepitaxial samples. For easier comparison among different substrate orientations, we highlight (in bold) the deposition conditions that were investigated on all the substrate orientations.

T_g (°C)	O-flux (sccm)	Growth rate[a] (nm/min)	rms (nm)	In incorporation (cm^{-3})
735	**0.33**	**≈0.65** [Figs. 1(b)–2(a)]	**2.45** [Fig. 1(a)]	**2×10^{19}** [Fig. 2(a)]
735—no MEXCAT	0.33	No growth	0.31	. . .
735	0.5	≈2.8	9.81	5×10^{20}
800	0.33	No growth	0.58	. . .
800	0.5	No growth	0.62	. . .
800	**0.75**	**≈2.2** [Fig. 3(a)]	**6.99** [Fig. 3(a)]	**1×10^{19}** [Fig. 3(a)]
800—no MEXCAT	0.75	No growth	1.08	. . .
800	1	≈3.3	23.30	1.5×10^{21}
900	**0.33**	**No growth**	**1.15**	. . .

[a]Full incorporation 3.3.
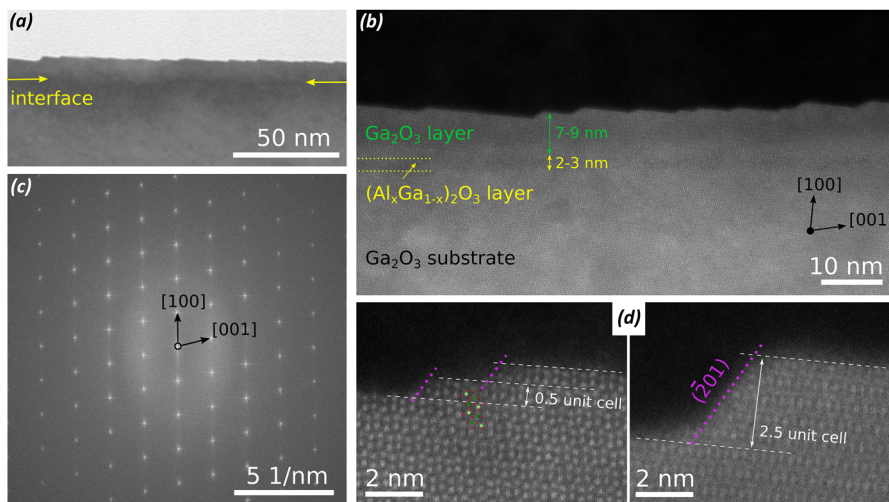
FIG. 5. (a) TEM bright field and (b) HAADF-STEM images acquired in cross section along the [010] direction of the In-catalyzed layer deposited at T_g = 800 °C with 0.75 sccm O-flux on top of a 6° offcut (100) substrate; yellow arrows and dotted lines are pointing toward the $(Al_xGa_{1-x})_2O_3$ marker layer. (c) FFT of a high resolution image (not shown) capturing both the layer and substrate; (d) high magnification STEM images of some surface steps with an overlayed Ga_2O_3 model structure, with the step edges facetted by $(\bar{2}01)$ planes indicated in purple.

orientation—i.e., T_g = 735 °C and O-flux = 0.33 sccm—did not result in layer growth on the (100) substrates. The AFM image of this tentative growth [Fig. 4(a)] shows the presence of a smooth surface (rms = 0.28 nm) with a morphology related to the 6° offcut along the c-direction,[9] and the ToF-SIMS profile highlights the absence of a layer [black dots in Fig. 4(e)].

Thus, we tested conditions that previously resulted in higher growth rates for $(\bar{2}01)$ homoepitaxy, i.e., T_g = 800 °C and O-fluxes ≥ 0.75 sccm. For these samples, an additional $(Al_xGa_{1-x})_2O_3$ interlayer was deposited at the substrate-film interface. The highest tested O-flux (2 sccm) resulted in a rough surface containing irregularly shaped islands with a typical height of about 150 nm [Fig. 4(d)], similar to the one previously discussed for the $(\bar{2}01)$-oriented layer deposited at 1 sccm. ToF-SIMS of this sample (not shown) suggests an almost full incorporation of the Ga-flux, with additional In-incorporation of about 21.4 cat. % (i.e., 65% of the total provided In-flux, $C_{In} \approx 8.2 \times 10^{21}$ cm^{-3}). Just for this sample, we detected an additional XRD reflection that we attribute to bixbyite In_2O_3 (not shown). The coexistence of both monoclinic and bixbyite phase in the $(In_xGa_{1-x})_2O_3$ alloy system is expected for such a large amount of In.[31,32]

A lower O-flux of 1 sccm resulted in a smoother surface (rms = 1.07 nm), with a morphology compatible with step bunching along the substrate offcut direction [Fig. 4(c)]. ToF-SIMS shows that the layer is ≈30 nm thick [green dots in Fig. 4(e)] with an estimated ≈2 nm thick $(Al_xGa_{1-x})_2O_3$ interlayer at the substrate interface. C_{In} as a function of depth is showing a similar trend as the one of thick layers, with a peak at the interlayer-layer interface ($C_{In} \approx 2.2 \times 10^{21}$ cm^{-3}, i.e. 5.7 cat. %) followed by a plateau region with limited In incorporation ($C_{In} \approx 2.2 \times 10^{18}$ cm^{-3}, i.e., 0.006 cat. %).

A further decrease in the O-flux to 0.75 sccm resulted in a smoother layer [rms = 0.32 nm, Fig. 4(b)] with a morphology resembling the one of the offcut substrate [Fig. 4(a)], and a thickness of 8–10 nm determined by ToF-SIMS [red dots in Fig. 4(e)]. Due to the limited thickness of the layer though, it is not possible to identify a clear plateau of C_{In} in the deposited layer; nonetheless, the C_{In} peak

at the interlayer-layer interface is ≈9.5 × 10^{19} cm^{-3} (i.e., 0.25 cat. %), while the lowest detected C_{In} in the layer is ≈3.5 × 10^{18} cm^{-3} (i.e. 0.01 cat. %). A deposition under the same conditions without In-flux did not result in a Ga_2O_3 layer growth, but just in a slight incorporation of In in the $(Al_xGa_{1-x})_2O_3$ marker layer [≈2 nm thick, see blue dots in Fig. 4(e)].

No extended defects are visible both in bright field and STEM images of the layer [Figs. 5(a) and 5(b), respectively]. The high crystal quality of the deposited layer is also apparent from the FFT image reported in Fig. 5(c), as no unexpected spots or streaks apart from the β-Ga_2O_3 ones are observed. Due to the Z-contrast in the HAADF-STEM image, the $(Al_xGa_{1-x})_2O_3$ interlayer can be identified as a dark line compared to the Ga_2O_3 substrate and layer. The respective thicknesses of the $(Al_xGa_{1-x})_2O_3$ and Ga_2O_3 layer are estimated to range between 2–3 and 7–9 nm [Fig. 5(c)], in good agreement with the SIMS results [red dots in Fig. 4(e)]. The step edges due to the 6°-offcut in the -c direction are resulting in $(\bar{2}01)$-planes[9] [purple dotted lines in Fig. 5(d)]. While the substrate surface presents only half-unit cell steps (≈0.62 nm), the layer surface presents steps of different heights as illustrated in the high-magnification STEM images in Fig. 5(d). All step heights correspond to multiples of half a unit cell in the a-direction, with the largest steps of 2.5 unit cells (≈3.1 nm). This points towards step bunching in some parts of the layer during growth, although this is not influencing the crystalline quality of the film.

As summarized in Table II, In-mediated MEXCAT is a fundamental ingredient to grow β-Ga_2O_3 layers on (100)-oriented substrates in the presence of an offcut along the c-direction. We have shown that the growth of high quality (100)-homoepitaxial layers is not just limited to MOVPE[9] but can be also extended to MBE.

MEXCAT on (001). We tested two deposition conditions that were previously investigated for the other two discussed orientations, i.e., T_g = 735 °C–O-flux = 0.33 sccm and T_g = 800 °C–O-flux = 0.75 sccm. The In-mediated growth run at the lowest T_g resulted in a ≈32 nm thick layer with a C_{In} peak at the substrate-layer interface of ≈7.5 × 10^{19} cm^{-3} (i.e., 0.19 cat. %) and a constant intralayer C_{In} of ≈1.1 × 10^{19} cm^{-3} (i.e., 0.03 cat. %) [Fig. 6(a)], highlighting a

TABLE II. Summary results for the (100) homoepitaxial samples on 6°-offcut substrates. We highlight (in bold) the deposition conditions that were investigated on all the substrate orientations.

| T_g (°C)	O-flux (sccm)	Growth rate[a] (nm/min)	rms (nm)	In incorporation (cm^{-3})
735	**0.33**	**No growth** [Fig. 4(e)]	**0.28** [Fig. 4(a)]	...
800	**0.75**	≈**0.27** [Figs. 4(e) and 5]	**0.32** [Figs. 4(b) and 5]	**4 × 10^{18}** [Fig. 4(e)]
800 – no MEXCAT	0.75	No growth	0.20	...
800	1	≈1 [Fig. 4(e)]	1.07 [Fig. 4(c)]	2.2 × 10^{18} [Fig. 4(e)]
800	2	≈3.3	59.60 [Fig. 4(d)]	8.2 × 10^{21}
900	**0.33**	**No growth**	**0.45**	...

[a]Full incorporation 3.3.

larger growth rate than on the $(\bar{2}01)$ and (100) orientations (about 20 nm and no growth, respectively, Tables I and II). The AFM micrograph of this layer [inset of Fig. 6(a)] shows (i) the presence of ≈100 nm large and ≈10 nm high dots on the surface whose origin is not currently understood, and (ii) elongated features along the [010] direction as already reported in other homoepitaxial growths on this orientation.[16,33] The resulting rms surface roughness is 3.11 nm.

For the growth at T_g = 800 °C and O-flux = 0.75 sccm, an approximately 2 nm thick $(Al_xGa_{1-x})_2O_3$ marker layer was intentionally deposited at the substrate-layer interface. The thickness of the β-Ga_2O_3 layer is estimated from ToF-SIMS as ≈65 nm, with a C_{In} peak at the substrate-layer interface of ≈1.1 × 10^{20} cm^{-3} (i.e., 0.29 cat. %) and a constant intralayer C_{In} of ≈3 × 10^{19} cm^{-3} (i.e., 0.08 cat. %) [Fig. 6(b)]. Under these deposition conditions, the layer is smooth (rms = 0.41 nm), still presenting elongated features oriented along the [010] direction [AFM in the inset of Fig. 6(b)]. The presence of well-defined XRD fringes in the vicinity of the (002) diffraction peak [facilitated by the $(Al_xGa_{1-x})_2O_3$ marker layer] allows us to precisely determine the thickness of the layer = 70 nm, i.e., 70% incorporation of the Ga total flux—growth rate = 2.3 nm/min [Fig. 6(c) red line], in line with the thickness range previously extracted from the SIMS profile [Fig. 6(b)]. Even though we are not maximizing the Ga-flux for our deposition runs, we highlight that the growth rate obtained here is exceeding what has been so far reported in the literature for this orientation with MBE

(≈0.9 nm/min).[16,33] A layer deposited under the same deposition conditions without additional In-flux resulted in no layer growth [black line in Fig. 6(c)].
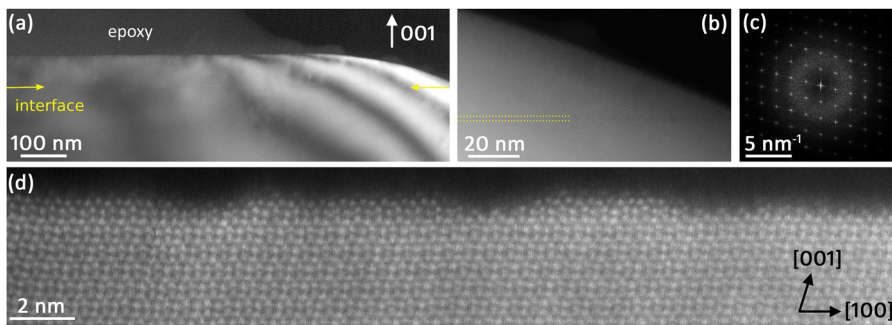
A cross-sectional TEM analysis along [010] of the In-catalyzed sample grown at T_g = 800 °C–O-flux = 0.75 sccm is reported in Fig. 7. The absence of contrast features in the dark field image in Fig. 7(a) (except for the TEM specimen thickness gradient related fringes) as well as the undisturbed appearance of the atomic pattern in high resolution STEM images [Figs. 7(b) and 7(d)] indicate a high crystalline quality of the film without extended defects (e.g., twinning, stacking faults), as can be also seen by the regular FFT as expected for perfect β-Ga_2O_3 [Fig. 7(c)]. The red arrows in Figs. 7(a) and 7(b) highlight the presence of the ≈2 nm thick $(Al_xGa_{1-x})_2O_3$ marker layer and the overall layer thickness of approximately 70 nm is confirmed. The surface of the layer appears smooth with a roughness peak-to-valley value of ≈1–2 c lattice parameters [i.e., 0.5–1 nm, Fig. 7(d)] in line with the AFM micrographs [inset of Fig. 6(b)]. The presence of elongated features along the [010] direction seems to be related to a partial faceting of the surface.

As summarized in Table III, we show that In-mediated MEXCAT allows us to obtain smooth (001) layers with a large incorporation of the provided Ga-flux with similar efficiency as previously reported for (010)[21] although at a lower substrate temperature. Our experiments suggest that (001) is a promising surface for β-Ga_2O_3 homoepitaxy because of the high quality of the deposited layers.
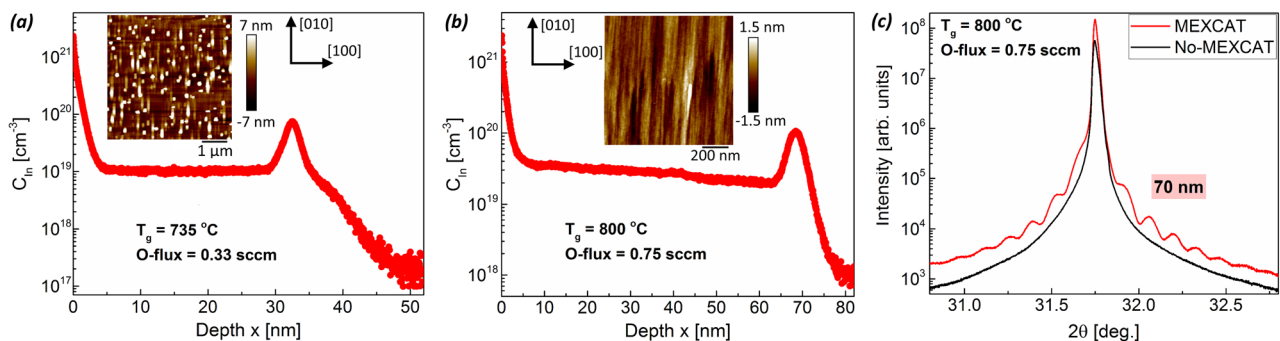
FIG. 6. C_{In} evaluated from ToF-SIMS measurements as a function of probed depth for (001) homoepitaxy at (a) T_g = 735 °C with an O-flux = 0.33 sccm and (b) T_g = 800 °C with an O-flux = 0.75 sccm; in the insets of the graphs, the respective AFM micrographs are shown. (c) (002) XRD peak of the samples deposited at T_g = 800 °C with an O-flux = 0.75 sccm with (red) and without (black) In-mediated MEXCAT.

FIG. 7. Cross-sectional TEM analysis along the [010] projection direction of the homoepitaxial (001) layer deposited at $T_g = 800\,^\circ$C with an O-flux = 0.75 sccm with MEXCAT [same as Fig. 6(b)]. (a) Dark field TEM and (b) HAADF-STEM images with yellow arrows and dotted lines pointing toward the $(Al_xGa_{1-x})_2O_3$ marker layer. (c) FFT of a high resolution TEM image (not shown here) capturing both layer and substrate. (d) High magnification HAADF-STEM image of the film surface.

It is important to highlight that the In-concentrations in the In-mediated MEXCAT deposited layers should not affect their electrical properties: In is energetically favorably replacing Ga in the octahedral site of the monoclinic cell,[31] and their isovalent nature excludes electrically active doping and ionized impurity scattering. We electrically characterized two unintentionally doped 50 nm thick Ga_2O_3 layers deposited with optimized In-mediated MEXCAT conditions on (001)- and (010)-oriented insulating substrates. Hg-contact capacitance-voltage measurements did not show any free carriers on both layers (even under forward bias the measured capacitance corresponded to the parasitic capacitance measured on an insulating glass slide). Additional 2-terminal current-voltage measurements between annealed Ti/Au contacts confirmed the presence of insulating layers (resistance >1 GΩ). These results confirm that, similar to Ga_2O_3 layers grown by MBE,[34] undoped Ga_2O_3 layers grown by MEXCAT-MBE are insulating. A separate dedicated study is needed to understand the interplay of the catalytic growth with n-type extrinsic doping, particularly with respect to the conflicting role of Sn as catalyst (i.e., not incorporated in the film)[24] and donor[10] during In-mediated MEXCAT.

From our results, it is clear that In-mediated MEXCAT allows us to widen the growth window on all the major substrate orientations (see Tables I–III). Nonetheless, there are visible differences in the growth rates Γ on the different β-Ga_2O_3 surfaces. Figure 8(a) allows for a direct comparison of Γ obtained with MEXCAT on different substrate orientations under three selected growth conditions as a function of their respective surface free energies from first principle calculations of Ref. 9.

Comparing the three sets of data collected in this work [blue, red, and green points Fig. 8(a)], we notice a monotonically increasing growth rate with increasing surface free energy of the different orientations, following the order $\Gamma(010) > \Gamma(001) > \Gamma(\bar{2}01) > \Gamma(100)$. We relate these experimental findings to the mechanism of the In-catalytic growth, which relies on the presence of In ad-atoms on the growth surface (i.e., Ga_2O_3) that can either form the catalyzing In_2O_3 (kinetically driven steps of the catalysis) or desorb off the surface. Once In_2O_3 is formed on the surface, its In atoms can be exchanged by Ga (thermodynamically driven step of the catalysis) forming Ga_2O_3 layer material and surface In ad-atoms that can re-enter the catalytic cycle or desorb. In the simple, quantitative, rate-equation based model for the In-mediated MEXCAT-MBE put forward in Ref. 23, the growth-rate limiting step is the thermally activated desorption of the In ad-atoms. Hence, the growth rate can be described as a function of all growth parameters [Eq. (6) in Ref. 23] and the activation energy Δ for In-desorption [Eq. (7) in Ref. 23] from the Ga_2O_3 surface. Providing the growth rate Γ observed in our experiments (and expressed in incorporated Ga-atoms per unit area and time) together with the used growth conditions (growth temperature T_g, In-flux Φ_{In}, Ga-flux Φ_{Ga}, and active O-flux for the oxidation of In to In_2O_3 Φ_O), we can use Eqs. (6) and (7) from Ref. 23 to calculate this activation energy as $\Delta = -k_B T_g \ln\{\text{sqrt}[\Phi_{In}{}^2\Phi_O(\Gamma^{-1} - \Phi_{Ga}{}^{-1})]/J_0\}$ with pre-exponential factor J_0 arbitrarily fixed at 10^{14} nm^{-2} s^{-1}.[23] The resulting values are shown in Fig. 8(b) as a function of surface free energy of the investigated Ga_2O_3 surface orientations. Larger Δ correspond to a larger barrier for the desorption of the In ad-atoms. Figure 8(b) shows that for given growth conditions, Δ increases with increasing surface free energy of the Ga_2O_3, suggesting that the stronger bonds/higher bond densities reflected by higher surface free energies also correspond to stronger bonds of this surface to the In ad-atoms. For example, the presence of low

TABLE III. Summary results for the (001) homoepitaxial samples. We highlight (in bold) the deposition conditions that were investigated on all the substrate orientations.

T_g (°C)	O-flux (sccm)	Growth rate[a] (nm/min)	rms (nm)	In incorporation (cm^{-3})
735	**0.33**	≈**1.1** [Fig. 6(a)]	**3.11** [Fig. 6(a)]	**1 × 10^{19}** [Fig. 6(a)]
800	**0.75**	≈**2.3** [Figs. 6(b), 6(c), and 7]	**0.41** [Fig. 6(b)]	**3 × 10^{19}** [Fig. 6(b)]
800 – no MEXCAT	0.75	No growth [Fig. 6(c)]	0.18	...
900	**0.33**	**No growth**	**0.17**	...

[a]Full incorporation 3.3.
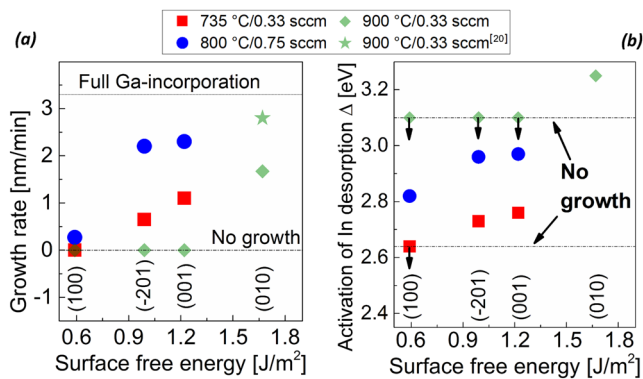
FIG. 8. (a) Growth rates obtained in this work for 6°-offcut (100), ($\bar{2}$01), (001), and (010) homoepitaxy by In-mediated MEXCAT-MBE under three different synthesis conditions [i.e., T_g = 735 °C–O-flux = 0.33 sccm (red), T_g = 800 °C–O-flux = 0.75 sccm (blue), and T_g = 900 °C–O-flux = 0.33 sccm (green)] and (b) activation energy of In desorption evaluated from the model of catalytic growth,[23] as a function of theoretically predicted surface energy[9] of the respective orientations. In (a), we also report the growth rate obtained in our previous study[21] on (010) homoepitaxy under similar conditions (star symbol). The black arrows in (b) mean that the data points (obtained by an assumed growth rate of 0.1 nm/min) are upper limits for the energy as these data points arise from samples without growth (i.e., a growth rate below 0.1 nm/min).

density/weak dangling bonds on a very stable surface such as the (100) results in an easier desorption of the In ad-atoms therefore not allowing their oxidation to form the In_2O_3 and thus no Ga_2O_3 formation by MEXCAT. While the absolute energies of Δ may be influenced by J_0, we note that their differences can provide experimental input for *ab initio* theory of the binding energy of In to the different Ga_2O_3 surfaces.

In conclusion, MBE homoepitaxial growth on all the major β-Ga_2O_3 substrate orientations is shown in this work. In-mediated MEXCAT is proven to fundamentally widen the deposition window of β-Ga_2O_3 on all of its native substrate orientations, neither forming ε/k-Ga_2O_3 nor incorporating large amounts of In (C_{In} < 0.1 c at. %). Notably, we highlight that the growth rate of the In-catalyzed layers deposited under the same synthesis conditions monotonically increases with the surface free energy of the used β-Ga_2O_3 substrate orientations according to $\Gamma(010) > \Gamma(001) > \Gamma(\bar{2}01) > \Gamma(100)$. We relate this behavior to an increasing binding energy of the In ad-atoms with increasing surface free energy. Moreover, we address fundamental differences on the obtainable structural quality of the layers deposited on different substrate orientations related to the growth mode and the crystal symmetry. Similar to the (100) orientation, the ($\bar{2}$01) one is a twinning plane in the monoclinic lattice; 2D nucleation and double positioning in this case leads to the formation of twin lamellae, low structural quality, and high surface roughness of the layers which might be mitigated by using substrates with proper offcut. Nonetheless, we demonstrate the possibility to obtain high quality thin films with In-mediated MEXCAT-MBE on the (001) and offcut (100) orientations, i.e., no structural defects and rms < 0.5 nm. Notably, in the case of (001) homoepitaxy, we demonstrate that In-mediated MEXCAT-MBE allows for similar growth rates to the ones obtainable on the widely

investigated (010) surface (2.3 nm/min, i.e., 70% incorporation of the impinging Ga-flux). In this regard, we would like to remark that the present work is not aiming at maximizing the absolute value of the growth rate, which could be scaled up with the provided metal and oxygen fluxes. Moreover, we demonstrate that the limited incorporation of In associated with MEXCAT-MBE depositions (10^{18}–10^{19} cm^{-3}) is not changing the insulating characteristics of unintentionally doped layers. Our experimental findings therefore suggest that (001) is a strong candidate for the homoepitaxial deposition of high quality layers on large area substrates. For practical purposes, future MEXCAT-MBE studies should aim at maximizing the growth rates, particularly on the (100) orientation, while maintaining a high crystalline quality.

REFERENCES

[1] S. J. Pearton, J. Yang, P. H. Cary, F. Ren, J. Kim, M. J. Tadjer, and M. A. Mastro, Appl. Phys. Rev. **5**, 011301 (2018).

[2] S. J. Pearton, F. Ren, M. Tadjer, and J. Kim, J. Appl. Phys. **124**, 220901 (2018).

[3] A. Kuramata, K. Koshi, S. Watanabe, Y. Yu, T. Masui, and S. Yamakoshi, Jpn. J. Appl. Phys., Part 1 **55**, 1202A2 (2016).

[4] Z. Galazka, R. Uecker, D. Klimm, K. Irmscher, M. Naumann, M. Pietsch, A. Kwasniewski, R. Bertram, S. Ganschow, and M. Bickermann, ECS J. Solid State Sci. Technol. **6**, Q3007 (2017).

[5] S. Geller, J. Chem. Phys. **33**, 676 (1960).

[6] G. Wagner, M. Baldini, D. Gogova, M. Schmidbauer, R. Schewski, M. Albrecht, Z. Galazka, D. Klimm, and R. Fornari, Phys. Status Solidi A **211**, 27 (2014).

[7] Z. Cheng, M. Hanke, Z. Galazka, and A. Trampert, Nanotechnology **29**, 395705 (2018).

[8] A. Fiedler, R. Schewski, M. Baldini, Z. Galazka, G. Wagner, M. Albrecht, and K. Irmscher, J. Appl. Phys. **122**, 165701 (2017).

[9] R. Schewski, K. Lion, A. Fiedler, C. Wouters, A. Popp, S. V. Levchenko, T. Schulz, M. Schmidbauer, S. Bin Anooz, R. Grüneberg, Z. Galazka, G. Wagner, K. Irmscher, M. Scheffler, C. Draxl, and M. Albrecht, APL Mater. **7**, 022515 (2018).

[10] K. Sasaki, A. Kuramata, T. Masui, E. G. Víllora, K. Shimamura, and S. Yamakoshi, Appl. Phys. Express **5**, 035502 (2012).

[11] M.-Y. Tsai, O. Bierwagen, M. E. White, and J. S. Speck, J. Vac. Sci. Technol., A **28**, 354 (2010).

[12] P. Vogt and O. Bierwagen, Phys. Rev. Mater. **2**, 120401 (2018).

[13] P. Vogt and O. Bierwagen, Appl. Phys. Lett. **109**, 062103 (2016).

[14] P. Vogt and O. Bierwagen, Appl. Phys. Lett. **106**, 081910 (2015).

[15] P. Vogt and O. Bierwagen, Appl. Phys. Lett. **108**, 072101 (2016).

[16] Y. Oshima, E. Ahmadi, S. Kaun, F. Wu, and J. S. Speck, Semicond. Sci. Technol. **33**, 015013 (2018).

[17] M. Baldini, M. Albrecht, A. Fiedler, K. Irmscher, R. Schewski, and G. Wagner, ECS J. Solid State Sci. Technol. **6**, Q3040 (2017).

[18] T. Zacherle, P. C. Schmidt, and M. Martin, Phys. Rev. B **87**, 235206 (2013).

[19] S. Lany, APL Mater. **6**, 046103 (2018).

[20] P. Vogt, A. Mauze, F. Wu, B. Bonef, and J. S. Speck, Appl. Phys. Express **11**, 115503 (2018).

[21] P. Mazzolini, P. Vogt, R. Schewski, C. Wouters, M. Albrecht, and O. Bierwagen, APL Mater. **7**, 022511 (2018).

[22] J. D. Blevins, K. Stevens, A. Lindsey, G. Foundos, and L. Sande, IEEE Trans. Semicond. Manuf. **32**, 466 (2019).

[23]P. Vogt, O. Brandt, H. Riechert, J. Lähnemann, and O. Bierwagen, Phys. Rev. Lett. **119**, 196001 (2017).

[24]M. Kracht, A. Karg, J. Schörmann, M. Weinhold, D. Zink, F. Michel, M. Rohnke, M. Schowalter, B. Gerken, A. Rosenauer, P. J. Klar, J. Janek, and M. Eickhoff, Phys. Rev. Appl. **8**, 054002 (2017).

[25]P. Vogt and O. Bierwagen, APL Mater. **4**, 086112 (2016).

[26]I. Cora, F. Mezzadri, F. Boschi, M. Bosi, M. Čaplovičová, G. Calestani, I. Dódony, B. Pécz, and R. Fornari, CrystEngComm **19**, 1509 (2017).

[27]T. Oshima, T. Okuno, N. Arai, Y. Kobayashi, and S. Fujita, Jpn. J. Appl. Phys., Part 1 **48**, 040208 (2009).

[28]R. Schewski, M. Baldini, K. Irmscher, A. Fiedler, T. Markurt, B. Neuschulz, T. Remmele, T. Schulz, G. Wagner, Z. Galazka, and M. Albrecht, J. Appl. Phys. **120**, 225308 (2016).

[29]D. Gogova, G. Wagner, M. Baldini, M. Schmidbauer, K. Irmscher, R. Schewski, Z. Galazka, M. Albrecht, and R. Fornari, J. Cryst. Growth **401**, 665 (2014).

[30]E. Ahmadi, O. S. Koksaldi, X. Zheng, T. Mates, Y. Oshima, U. K. Mishra, and J. S. Speck, Appl. Phys. Express **10**, 071101 (2017).

[31]M. B. Maccioni, F. Ricci, and V. Fiorentini, Appl. Phys. Express **8**, 021102 (2015).

[32]S. Bin Anooz, A. Popp, R. Grüneberg, C. Wouters, R. Schewski, M. Schmidbauer, M. Albrecht, A. Fiedler, M. Ramsteiner, D. Klimm, K. Irmscher, Z. Galazka, and G. Wagner, J. Appl. Phys. **125**, 195702 (2019).

[33]S.-H. Han, A. Mauze, E. Ahmadi, T. Mates, Y. Oshima, and J. S. Speck, Semicond. Sci. Technol. **33**, 045001 (2018).

[34]M. H. Wong, K. Sasaki, A. Kuramata, S. Yamakoshi, and M. Higashiwaki, Appl. Phys. Lett. **106**, 032105 (2015).